Available online at www.sciencedirect.com
ScienceDirect
Trans. Nonferrous Met. Soc. China 34(2024) 3471−3485
Transactions of Nonferrous Metals Society of China
www.tnmsc.cn

Structure-controlled slow dynamics in Al−Mg melts

Fei-qi HUANG[1,2], Xiao-dan WANG[1], Lin-si-tong HUANG[1], Ju-rui MA[1], Yu-jun JIANG[1], Hua-shan LIU[1], Jin-liang HU[2], Hai-long PENG[1], Bo ZHANG[2]

1. School of Materials Science and Engineering, Central South University, Changsha 410083, China;
2. Space Materials Team, Songshan Lake Materials Laboratory (SLAB), Dongguan 523808, China

Received 30 June 2024; accepted 21 October 2024

Abstract: Molecular dynamics simulation was employed to investigate the dynamical and structural properties of Al−Mg melts with the Al concentration systematically changed. The results show that the viscosity of $Al_{67}Mg_{33}$ abnormally surpasses that of $Al_{85}Mg_{15}$ below 550 K, inconsistent with the tendency at high temperatures. The evolution of the icosahedral order population is found to account for this dynamic behavior. Structural analysis shows a preferred bonding between Al and Mg atoms in the nearest neighbor shells, while a repelling tendency between them in the second shells, leading to the prepeak emergence in the partial static structure factors. The formation of icosahedral clusters is constrained in the Al-rich compositions because of the lack of sufficient Mg atoms to stabilize the clusters geometrically. These results demonstrate the structural consequence through the interplay between geometric packing and chemical interaction. These findings are crucial to understanding the structure−dynamic properties in Al−Mg melts.

Key words: Al−Mg melt; slow dynamics; chemically ordered structure; topologically ordered structure; molecular dynamics simulation

1 Introduction

Al−Mg alloys attract considerable attention in the automotive and aerospace industries due to the high specific strength [1,2]. Al−Mg-based alloys perform exceptionally well in marine and humid environments, which makes them widely used in shipbuilding and marine engineering [3,4]. Al−Mg metallic glasses (MGs) can be obtained by rapidly quenching the melts to avoid crystallization. Al−Mg MGs possess many unique properties, particularly exhibiting superior mechanical properties and corrosion resistance compared to their crystalline counterparts [5]. However, the glass-forming ability (GFA) of Al−Mg MGs is relatively poor, which has been a challenge in materials science for the past 40 years [6]. Studying the structure and dynamics of supercooled liquids can provide insights into the vitrification process, offering new perspectives for improving the GFA of Al−Mg MGs [7−9].

The microstructure determines the material properties [10,11]. In MGs, the structure is inherited from the liquid state, with key features being liquid-like regions and string-like relaxation processes [9]. The microscopic structure of liquids mainly refers to various types of short-range order (SRO). This includes the topological SRO that describes local geometric packing, and the chemical SRO that describes the distribution of different atomic species. Chemical order and topological order are interrelated and influence each other; they interplay with each other and ultimately influence the dynamical properties of the liquids [12].

Corresponding author: Jin-liang HU, E-mail: hujinliang@sslab.org.cn;
Hai-long PENG, E-mail: hailong.peng@csu.edu.cn
DOI: 10.1016/S1003-6326(24)66620-3

In Al-based melts, strong chemical effect often presents. The preferred chemical bonding between different atomic pairs leads to the formation of chemical SRO in these melts [13,14]. The prepeaks observed in the static structure factors can characterize the chemical effects in the liquids [15]. The prepeaks have been reported in many Al-based binary melts both in experiments and computer simulations. For instance, they have been observed in Al−Au melts by classical molecular dynamics simulations [16], in Al−Cu melts by ab initio calculations [13], and in $Al_{80}Ni_{20}$ melts by neutron diffraction experiments [17]. Chemical concentration fluctuations in adjacent atomic shells at low temperatures could cause the appearance of prepeaks [18]. However, the specific structural characteristics responsible for the appearance of prepeaks remain unclear.

Atomic clusters can influence the hardening process of alloys [19,20], such as Cu−Mg clusters in Al−Cu−Mg alloys and Mg−Si clusters in Al−Mg−Si alloys [21−25]. It is analogous for the role played by the topological order structures on the dynamics in Al-based melts. In $Al_{60}Cu_{40}$ melts, no single type of cluster predominates [26]. In contrast, in Al−Mg melts, icosahedral clusters centered around Al atoms dominate [27]. These icosahedral clusters inhibit crystallization of Al−Mg melts and play a crucial role in forming MGs [28]. Furthermore, these icosahedral clusters are inter-connected through four types of atomic sharing, forming a medium-range order (MRO) [29]. The anomalous ordering transitions occurring in undercooled Al_3Zr liquid involve the following two stages: directional diffusion and defect cluster stabilization [7]. This significantly enhances the filling efficiency of Al-rich regions, thereby reducing the Gibbs free energy of the entire system.

Liquid dynamics plays a crucial role in the solidification and crystal growth processes, as the solute concentration and its diffusion rate in the liquid phase influence the rate and morphology of crystal growth, ultimately impacting the alloy's performance [30−33]. For example, in 7xxx series Al alloys, Zn and Mg concentrations and diffusion affect $MgZn_2$ (η) phase distribution, where high concentrations can reduce fracture toughness and corrosion resistance. By controlling solute diffusion, a finer η phase improves mechanical properties [34]. The impact of structure on dynamics in liquids has been a topic of ongoing interest, particularly concerning the slow dynamics in glass-forming liquids. Notable phenomena include the violation of the Stokes−Einstein (SE) relationship and non-Arrhenius transitions [35−37]. Chemical interaction influences the dynamic collectivity in liquids, resulting in strong coupling between the diffusion coefficients of the chemically interacting elements [15,16]. In Cu−Ag melts, the anomalous dynamic behavior resulting from changes in the diffusion mechanism originates from a rapid increase in the number of slow-moving particles and a sudden expansion in the local structural differences between atoms [38]. In Al−Ni melts, the strong interaction between icosahedral SRO and chemical SRO results in a pronounced peak in the interdiffusion coefficient near the equiatomic composition [14]. However, detailed studies linking structure with dynamics in the Al−Mg system have not yet conducted.

We employed classical molecular dynamics (MD) simulations to investigate the dynamic properties and structure of Al−Mg melts, with the Al molar fraction of x_{Al}=0, 15%, 33%, 50%, 67%, 85%, and 100%. This work represents a significant advancement in understanding the interplay between geometric and chemical ordering in Al−Mg melts, providing new insights into the mechanisms that govern their dynamic properties. We calculated the diffusion coefficients and viscosity among other dynamic properties of the Al−Mg melts, revealing an anomalous phenomenon where $Al_{67}Mg_{33}$ surpasses $Al_{85}Mg_{15}$ in viscosity at low temperatures. Combining the analysis of chemical ordering and topological ordering structures, we elucidated the close relationship between the structure and dynamics of Al−Mg melts. We revealed the structural origins behind slow dynamic phenomena, including the temperature evolution of transport coefficients and the abnormal composition dependence. This is significant for understanding the glass-forming process in the Al-based alloys.

2 Methods

2.1 Simulation details

We employed the large-scale atomic/molecular massively parallel simulator (LAMMPS) to conduct classical MD simulations on the Al−Mg

glass-forming liquids based on the embedded atom method (EAM) potential [39]. The potential function used was developed by LIU and ADAMS [40] for Al−Mg alloys, where the total energy (E_{tot}) can be expressed as

$$E_{tot}=\sum_i F_\alpha^i(\rho_i)+\frac{1}{2}\sum_{i\neq j}\phi_{\alpha\beta}(r_{ij}) \quad (1)$$

where F is the embedding energy, ρ_i is the electron density at atom i, ϕ is a pair potential interaction, α and β are the element types of atoms i and j, respectively, and r_{ij} is the distance between atoms i and j. The electron density at atom i was calculated as $\rho_i=\sum_{j\neq i} f_{\alpha\beta}(r_{ij})$, where $f_{\alpha\beta}(r)$ designates the electron density generated by element type β at distance r from a central atom of type α.

For the Al−Mg liquids, we performed MD simulations with 5000 atoms under periodic boundary conditions. A system consisting of 5000 atoms is a reasonable compromise, providing sufficient statistics while allowing calculations to be completed within an acceptable time scale. The periodic boundary conditions were employed to avoid boundary effects and simulate the behavior of a bulk system. The variable x_{Al} represents the molar fraction of Al atoms in the Al−Mg liquids. The compositions studied include: x_{Al}=0, 15%, 33%, 50%, 67%, 85%, and 100%. The computer simulations started from a random configuration at 1600 K with a time step of 1 fs. After relaxation for 50000 time steps, the system reached equilibrium. Subsequently, it was cooled down to the target temperature at a rate approximately 2.5×10^{12} K/s in the NPT ensemble (constant number of particles, pressure, and temperature). For x_{Al}=15%, 33%, 50%, 67% and 85%, the lowest temperature studied was 530 K, while for pure Al and pure Mg, it was 580 K. At the target temperature, the box length was set to the value at zero pressure, and configurations were collected using the NVT ensemble (constant number of particles, volume, and temperature). The running time increased as the temperature decreased, ensuring that the equilibrium state reached at low temperatures. Sixteen independent runnings were conducted at each composition and temperature to make statistical averages.

2.2 Calculation of liquid dynamics

Dynamic properties of the melts including atomic diffusion, shear viscosity, and dynamic heterogeneity were calculated. According to the Einstein equation, the diffusion coefficient (D) can be measured from the mean-square displacement (MSD):

$$D=\lim_{t\to\infty}\frac{1}{6t}\langle\Delta r^2(t)\rangle \quad (2)$$

where $\langle\Delta r^2(t)\rangle$ represents the MSD, defined as

$$\langle\Delta r^2(t)\rangle=\frac{1}{N}\langle\sum_{i=1}^{N}[\vec{r}_i(t)-\vec{r}_i(0)]^2\rangle \quad (3)$$

with N the number of atoms and $\vec{r}_i(t)$ the position of atom i at time t.

Viscosity (η) was calculated via the Green−Kubo relation [41]:

$$\eta=\frac{V}{k_BT}\int_0^\infty\langle P_{xy}(t)P_{xy}(0)\rangle dt \quad (4)$$

where P_{xy} is the off-diagonal elements of the stress tensor and V is the volume of simulated cubic box, k_B is the Boltzmann constant and T is the temperature.

The non-Gaussian parameter ($\alpha_2(t)$) was calculated to quantify the dynamic heterogeneity in the melts [42], defined as

$$\alpha_2(t)=\frac{3\langle\Delta r^4(t)\rangle}{5\langle\Delta r^2(t)\rangle^2}-1 \quad (5)$$

where $\langle\Delta r^4(t)\rangle$ is the mean-quadruple displacement.

2.3 Calculation of liquid structures

To explore the relationship between the dynamics and structure of Al−Mg melts, chemical order structure and topological order structure in the melts were characterized. Partial static structure factors ($S_{\alpha\beta}(q)$) were calculated through the Fourier transformation of the partial pair distribution function, $g_{\alpha\beta}(r)$, in the liquids:

$$S_{\alpha\beta}(q)=\delta_{\alpha\beta}+\frac{\sqrt{N_\alpha N_\beta}}{V}\cdot\int_V 4\pi r^2[g_{\alpha\beta}(r)-1]\frac{\sin(qr)}{qr}dr \quad (6)$$

where q is the magnitude of the wave vector; $\delta_{\alpha\beta}$ is the Kronecker delta symbol, which equals 1 when $\alpha=\beta$ and 0 when $\alpha\neq\beta$; N_α and N_β are the numbers of atoms of types α and β, respectively.

Local structures of Al−Mg melts were studied based on the Voronoi tessellation method [43,44].

This method divides the system space into Voronoi polyhedra around each atom, with each polyhedron defined by perpendicular planes connecting the central atom and all its neighboring atoms. The types of Voronoi polyhedra are described by the index $\langle n_3, n_4, n_5, n_6\rangle$, where n_i denotes the number of i-edged faces of the Voronoi polyhedron [45]. For example, $\langle 0,0,12,0\rangle$ represents a perfect icosahedron with 12 pentagonal faces.

The local five-fold symmetry (LFFS) was utilized to quantify Voronoi polyhedra clusters [46], defined as the fraction of pentagonal faces in the polyhedron (f_i^5):

$$f_i^5 = n_i^5 \Big/ \sum_{\kappa=3,4,5,6} n_i^{\kappa} \tag{7}$$

where n_i^{κ} denotes the number of κ-edged polygon in Voronoi polyhedron type i.

The structural parameter (d_5) was used to quantify the average degree of five-fold symmetry in Al−Mg melts [47]:

$$d_5 = \sum_i \left(f_i^5 P_i \right) \tag{8}$$

where P_i denotes the proportion of Voronoi polyhedra type i.

To quantify the icosahedral order in Al−Mg melts, the bond orientational order (BOO) parameters developed by STEINHARDT et al [48] are introduced. The local structure of particle i was characterized by the BOO parameters defined as follows:

$$Q_l(i) = \sqrt{\frac{4\pi}{(2l+1)} \sum_{m=-l}^{l} |Q_{lm}(i)|^2} \tag{9}$$

$$\hat{W}_l(i) = \frac{W_l(i)}{\left[\sum_{m=-l}^{l} |Q_{lm}(i)|^2 \right]^{3/2}} \tag{10}$$

with

$$Q_{lm}(i) = \frac{1}{n(i)} \sum_{j=1}^{n(i)} Y_{lm}(r_{ij}) \tag{11}$$

$$W_l = \frac{\sum_{m_1+m_2+m_3=0}^{m_1,m_2,m_3} \begin{bmatrix} l & l & l \\ m_1 & m_2 & m_3 \end{bmatrix} Q_{lm_1} Q_{lm_2} Q_{lm_3}}{\sum_{m=-l}^{l} |Q_{lm}(i)|^2} \tag{12}$$

where $n(i)$ is the coordination number of particle i; $Y_{lm}(r_{ij})$ denotes the spherical harmonics; l is an integer; m ranges from $-l$ to l. A combination of the order parameters Q_6, $\hat{W}_6$ and $\hat{W}_4$ can be used to identify the symmetry of local positional order. Using this method, we can determine the proportions of atoms with fcc-like, hcp-like, bcc-like, and local icosahedral order.

3 Results and discussion

3.1 Liquid dynamics

In this section, we reported the dynamic properties of Al−Mg glass-forming liquids, such as self-diffusion coefficients, viscosity, and the Stokes−Einstein (SE) relation that links them. This aids in understanding the GFA and stability of glass-forming liquids. One instance is that the low dynamics can hinder the crystallization process, and then benefits GFA.

Figure 1 shows the temperature evolution of diffusion coefficients and viscosity for different

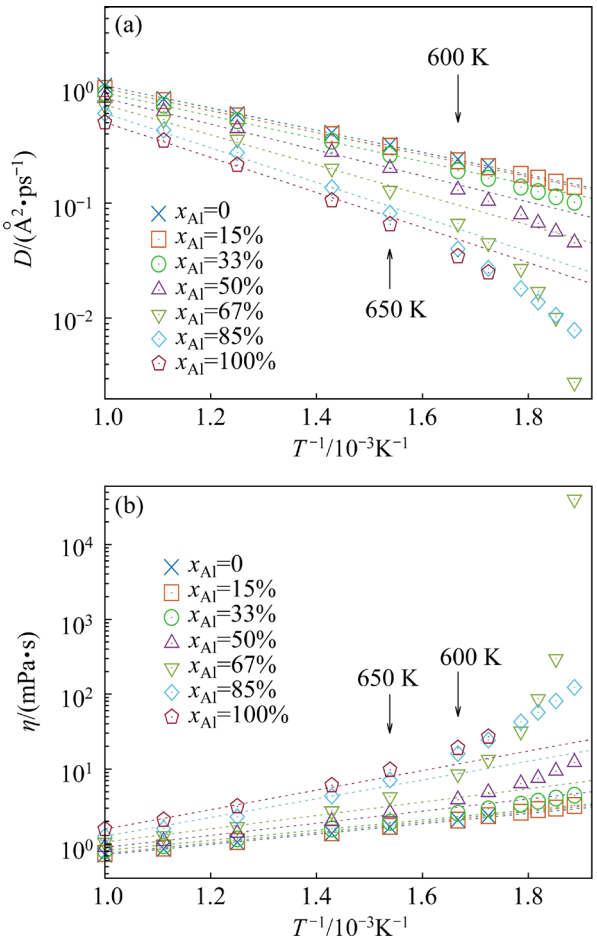

Fig. 1 Temperature evolution of diffusion coefficient (a) and viscosity (b) in Al−Mg liquids (The dotted line represents the fitting of the Arrhenius relation at high temperatures)

components of the Al−Mg liquids. As the compositions of pure Al and pure Mg crystallize below 580 K, the data for pure elements below this point are not available. At high temperatures, D decreases with increasing Al concentration, while it increases for η. This can be understood as the mixing of Mg liquids with more viscous Al liquids.

Temperature evolution of transport coefficients can be considered as a thermal activation process described by the Arrhenius law: $A=A_0\exp[-E_a/(RT)]$, with $A=D$ or $1/\eta$, and E_a the activation energy associated with a group of atoms within a certain volume during the thermal activation process. The Arrhenius law describes the data well at high temperatures (see dotted lines in Fig. 1). It fails in the temperature range investigated for most of the compositions. The non-Arrhenius transition indicates that the activation energy E_a is not constant but increases with the increase of the undercooling. The associated activation volume also increases. Thus, more atoms are involved in the transport processes. This is a signature of the emergence of collective motion in glass-forming liquids, and has been reported in various liquids [8,15,18]. No clear non-Arrhenius transition can be seen in compositions for x_{Al}=0 and 15%. The onset points for the non-Arrhenius transition are at about 600 K for x_{Al}=33% and 50%, while they are at about 650 K for x_{Al}=67%, 85%, and 100%. This could be due to the geometrical packing discrepancy in these compositions. Icosahedral clusters that stabilize supercooled liquids are responsible for the dynamics slowing down in the melts. The population of these clusters is consistently found to increase with the increase of x_{Al}, accounting for the composition-dependent onset point of the non-Arrhenius transition.

One notable and interesting phenomenon is that the dynamics of $Al_{67}Mg_{33}$ becomes the lowest at low temperatures. This can be seen both in D and η: a drastic drop appears in D, while a sharp increase appears in η, as shown in Figs. 1(a) and (b). This phenomenon occurs at temperatures below 550 K. This is a non-entropic mixing effect. Some anomalous structural transitions at low temperatures may be the cause of this slow dynamic behavior.

Self-diffusion coefficients and viscosity are correlated through the SE relation, expressed as $D\eta=k_BT/(2\pi d)$, where d is the effective atomic diameter. The SE relation was initially applied to the diffusion of macroscopic particles in solvents composed of much smaller constituents. However, it was also applied to dense liquids, linking the self-diffusion of larger components with the viscosity of the liquids [49]. The temperature evolution of $1000D\eta/T$ using different self-diffusion coefficients is shown in Fig. 2. The SE relation holds at high temperatures, while it breaks down at low temperatures. The degree of deviation from the SE relation calculated using the self-diffusion coefficients of Al and Mg atoms differs, with the deviation being more pronounced when using the D_{Al}. This is because the diffusivity of Al is higher than that of Mg. However, the temperature at which the breakdown of the SE relation occurs is the same. The SE relation weakly breaks down at about 600 K for x_{Al}=50%, while at about 650 K for x_{Al}=67% and 85%. The breakdown of SE relation is ascribed to the emergence of collective motion in viscous liquids. This can be confirmed by the fact that the breakdown points coincide with the onset points of the non-Arrhenius transition found in the transport coefficients.

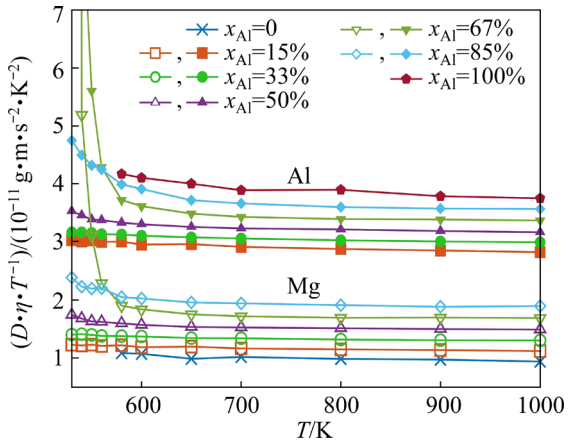

Fig. 2 SE relation with temperature for Al (full-filled symbols) and Mg atoms (open symbols)

Breakdown of the SE relationship is one of the hallmarks for the emerging slow dynamics in viscous liquids, connected with the celebrated finding in glass transition, i.e., the so-called dynamic heterogeneity [50,51]. The dynamic heterogeneity is the phenomenon that the connectivity of atomic motions fluctuates both in time and space. One of the convenient methods to quantify the dynamic heterogeneity in time is to calculate the non-Gaussian parameters.

Figure 3 shows the non-Gaussian parameters, $\alpha_2(t)$, for different components at 540 and 600 K. At short time, the displacement of atoms is proportional to the thermal velocity, which gives zero value of $\alpha_2(t)$. With increasing time, non-Gaussian statistics increases due to the collective motion between atoms. At long-time limit, atomic motion reaches the diffusion regime, making $\alpha_2(t)$ approach zero again. Thus, a maximum peak emerges in $\alpha_2(t)$, where the collective motion between atoms is the strongest. Generally, the maximum value increases with the increase of Al concentration. This implies that the dynamic heterogeneity increases with the increase of x_{Al}. The maximum value for x_{Al}=85% is the highest at 600 K, while it is the highest for x_{Al}=67% at 540 K. This is well consistent with the highest viscosity or the lowest diffusivity compositions found at these two temperatures (see Fig. 1).

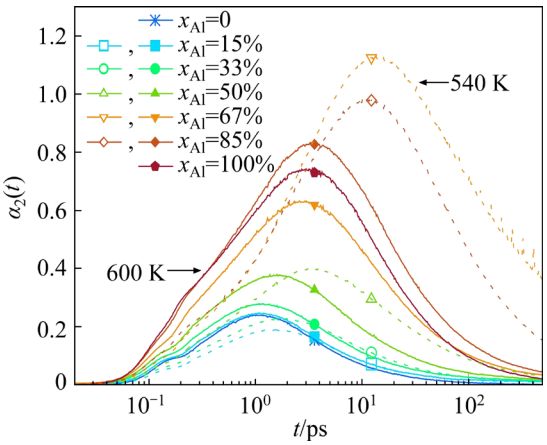

Fig. 3 Non-Gaussian parameters for different compositions at 600 K (solid line) and 540 K (dashed line)

To better illustrate the temperature dependence of dynamic heterogeneity, we calculated the variation of the maximum non-Gaussian parameter, α_2^{max}, and its temperature derivative, $d\alpha_2^{max}/dT$, in the three compositions where the SE relation exhibits strong violation at low temperatures, as shown in Fig. 4. α_2^{max} is small at high temperatures and increases with decreasing temperature, indicating a growth of dynamic heterogeneity. This trend is similar to that of $D\eta/T$, where the extent of the violation of the SE relationship also increases with lowering temperature. The derivative, $d\alpha_2^{max}/dT$, gives the speed of the changing dynamic heterogeneity. At T>700 K, $d\alpha_2^{max}/dT$ is nearly constant, while it decreases rapidly below 700 K. This indicates that the dynamic heterogeneity of these three components increases rapidly below 700 K, a temperature close to the weak breakdown point of the SE relationship. The rapid increase in dynamic heterogeneity also suggests a transition of the atomic motion towards collective motion.

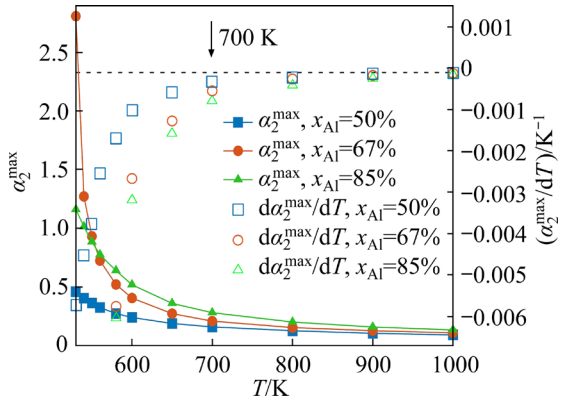

Fig. 4 Maximum non-Gaussian parameter (α_2^{max}) and temperature derivative in compositions x_{Al}=50%, 67%, and 85%

A consistent phenomenon can be observed in the temperature evolution of α_2^{max} and $d\alpha_2^{max}/dT$: the maximum non-Gaussianality of x_{Al}=67% composition exceeds that of x_{Al}=85% composition, so does the change rate of the maximum non-Gaussianity. This coincides with the findings in viscosity or diffusivity (Fig. 1). Therefore, the abnormal change of the dynamics with composition could be connected to the change of the dynamic heterogeneity in the Al−Mg melts. Despite the clue of dynamic heterogeneity found for the abnormal behavior of transport coefficients, the structural significance for it is still unclear and needs to be clarified.

3.2 Chemically ordered structure

Previous studies have indicated that in Al-based melts, there often exists strong chemical interaction. Chemical effects arise from electronic interactions and can influence the structure and dynamic properties of the liquid [13,14]. The emergence of prepeaks in the static structure factor $S(q)$ is one of the most outstanding features for the occurrence of chemical effects, and is measurable in experiments.

Figure 5 shows the calculated partial $S(q)$, for different compositions at 600 K. Prepeaks are

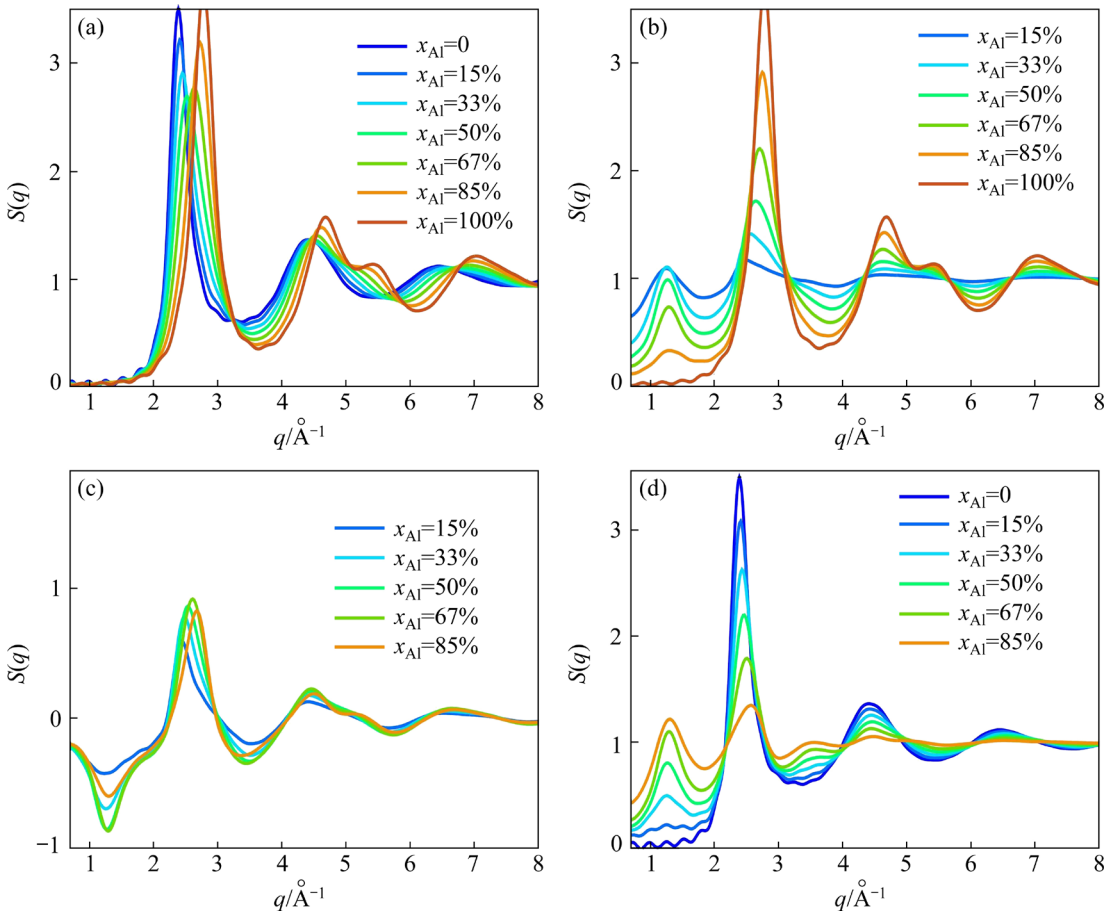

Fig. 5 Total (a) and partial static structure factors $S(q)$ for Al−Al (b), Al−Mg (c), and Mg−Mg (d) pairs at 600 K in Al−Mg melts

observed in both $S_{AlAl}(q)$ and $S_{MgMg}(q)$ (Figs. 5(b) and (d)). Prepeaks in Al-rich compositions appear more strongly in $S_{MgMg}(q)$, whereas they strongly appear in $S_{AlAl}(q)$ for the Mg-rich compositions. The prepeak is more likely to occur in the minority pairs of $S(q)$. In $S_{AlMg}(q)$, however, negative prepeaks emerge, which counteract the prepeaks in $S_{AlAl}(q)$ and $S_{MgMg}(q)$, resulting in the absence of prepeaks in the total $S(q)$. The emergence of prepeaks indicates a change in the filling behavior of secondary coordination shells, which is a reflection of chemical ordering in the liquid, as reported in Al−Fe [52], Zr−Ni [53], Al−Au [16], Al−Cu [13], Al−Ni [17], and Al−Ti [18] melts. However, the specific structures responsible for the chemical ordering remain elusive. As the prepeaks in the partial $S(q)$ become sharper with decreasing temperature, studying the structural changes in the liquid with temperature variation can provide an explanation for the occurrence and enhancement of the prepeaks.

The chemical environment in the atomic coordination shells can be quantified by the partial coordination number, which can be obtained from the integration of the partial pair distribution function $g_{\alpha\beta}(r)$:

$$Z_{\alpha\beta} = 4\pi\rho c_\alpha \int_{r_1}^{r_2} r^2 g_{\alpha\beta}(r)\mathrm{d}r \tag{13}$$

where $Z_{\alpha\beta}$ represents the number of species α surrounding a central species β, c_α is the concentration of species α, and ρ is the average number density. When computing the first coordination shells, r_1 is zero, and r_2 is the position of the first valley in the partial radial distribution function. When computing the second coordination shells, r_1 is the position of the first valley in the partial radial distribution function, and r_2 is the position of the second valley in the partial radial distribution function. The total coordination number

of atomic species β is given by $Z_\beta = \sum_\alpha Z_{\alpha\beta}$. If the atoms in the coordination shell around a central atom are randomly distributed according to the liquid concentration, the ratio of coordination species is: $Z_{\alpha\beta}/Z_\beta = c_\alpha$, independent on the species of the central atom.

We calculated the discrepancies of the ratio of coordination species in the first and second coordination shells to the random distribution, i.e., $Z_{\alpha\beta}/Z_\beta - c_\alpha$, with the results shown in Fig. 6. In the first coordination shells, we observed that the number of neighboring Al atoms around a central Al atom is fewer than that expected from random distribution (Fig. 6(a)). This indicates that the Al atoms avoid being nearest neighbors of themselves. As a counterbalance, the concentration of Mg atoms around central Al atoms will be higher than that expected from random mixing, with the value opposite to that of Al (the results are not shown here). Interestingly, the avoidance of the Al−Al connection is weaker in non-equiatomic compositions (x_{Al}=15%, 85%), but it is stronger in compositions close to the equiatomic one (x_{Al}=33%, 50%, 67%). For the local chemical environment around Mg atoms, we found a clear excess Al concentration at x_{Al}=67% and 85% (Fig. 6(b)). This implies the preferred connection between Al and Mg atoms in these compositions. With decreasing temperature, the avoidance for Al−Al pairs and the preferred connection for Al−Mg pairs gradually increase. Thus, the chemical interaction or the chemical short-range order is strengthened at low temperatures. This supports the previously mentioned non-entropic mixing effect observed at low temperatures.

The emergence of the prepeaks in $S(q)$ correlates with the structures beyond the first coordination shells. To this end, we investigated the coordination numbers of the second coordination shells. Figures 6(c) and (d) show the results obtained for central Al and Mg atoms, respectively. The fluctuations are larger than those in the first coordination shells, but the trend can still be observed. The number of Al atoms around central

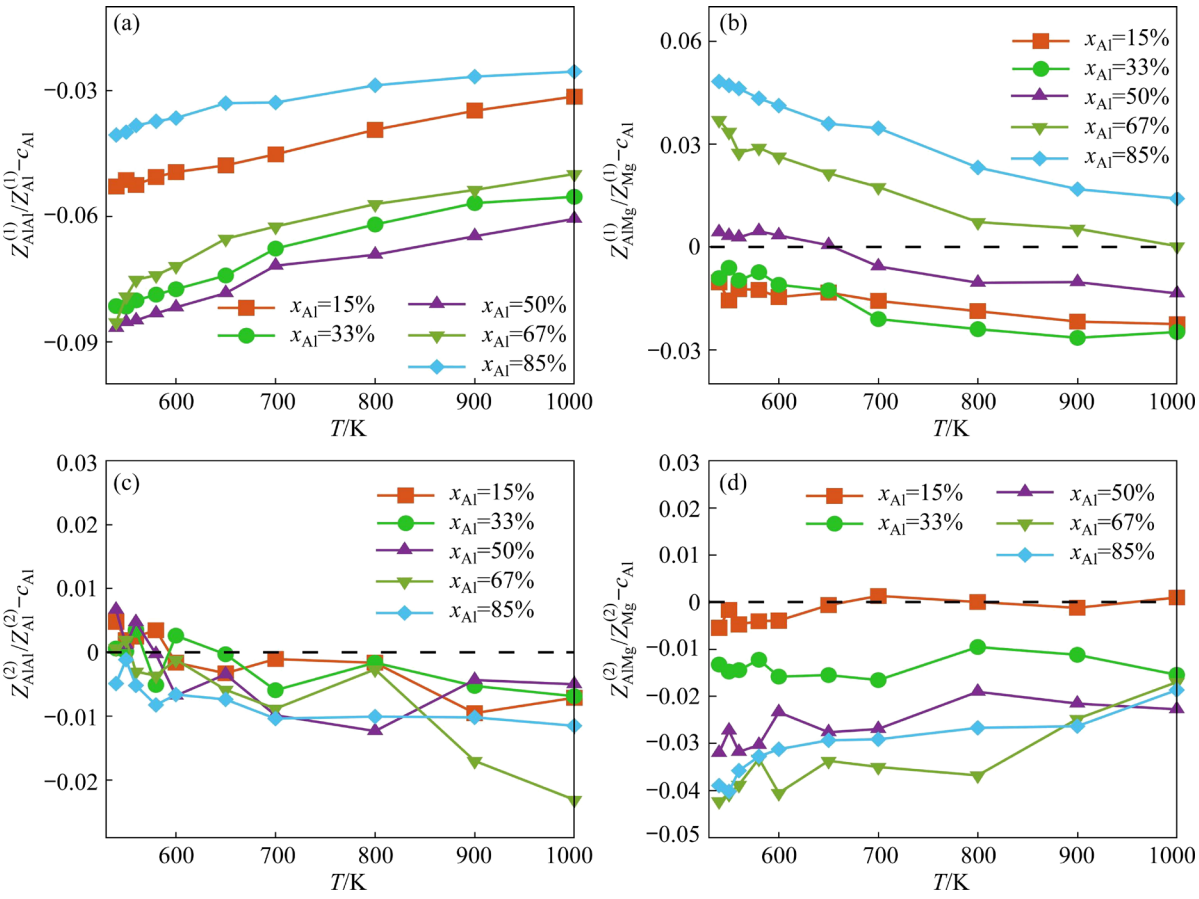

Fig. 6 Ratios of coordinating numbers relative to concentration expected from random mixing in first neighborhoods around central Al atoms (a), and Mg atoms (b); and in second neighborhoods around Al atoms (c), and Mg atoms (d)

Al atoms in the second coordination shells is slightly lower than that expected from random distribution. As the temperature decreases, the preference of central Al atoms for Al atoms increases, eventually to the value of randomly mixing. Thus, the Al atoms are slightly repelled around the central Al atoms in the second neighbor shells, similar to the situation of the first neighbor shells. However, one should note that the repelling effect is much weaker in the second neighbor shells than that in the first neighbor shells (Fig. 6(a)). This can induce a concentration fluctuation around the central Al atoms in the neighboring shells, leading to the emergence of the prepeaks observed in Fig. 5(b).

The repelling effect is more clearly observed in the second neighbor shells around Mg atoms (Fig. 6(d)); Mg-coordinating Al atoms are fewer than that expected in random mixing in the compositions except for x_{Al}=15% melts. This is opposite to the case in the first shells, where Al and Mg atoms prefer to be the nearest neighbors. The less Al coordinates in the second neighbor shells of Mg atoms may be the consequence of the repelling effect among Al atoms. As Al atoms avoid being nearest neighbors of themselves, Al atoms in the first shells could depress the occurrence of other Al atoms in the second shells around Mg. The opposite trends between the first and second coordination shells exhibit a unique alternating excess concentration fluctuation phenomenon, which gradually strengthens as the temperature decreases. Similar phenomena have also been reported in Al−Ti melts [18]. The alternating excess concentration fluctuations can lead to the appearance of more notable prepeaks in $S(q)$ in Mg−Mg pairs observed in Fig. 5(d).

3.3 Topologically ordered structure

The topological short-range order plays a nontrivial role in dynamical properties of metallic liquids. The type of topological SRO is closely related to the geometric packing efficiency. It has been reported that there is a large amount of icosahedral order in Al−Mg melts [27−29,54]. This is because icosahedral clusters are the densest and energetically favorable clusters [55]. The effective atomic size ratio of Al to Mg atoms is 0.894, close to the ideal effective atomic size ratio of icosahedral packing, which is 0.902 [56]. To compare with the dynamical behavior, we replotted the viscosity as shown in Fig. 7(a), which is the same as that presented in Fig. 1(b). The icosahedral order in Al−Mg melts was quantified using the average degree of five-fold symmetry (Fig. 7(b)) and the local icosahedral (ICO) order fraction obtained from BOO parameter analysis (Fig. 7(c)). Additionally, Fig. 7(d) presents the variation of the fraction of the eight most abundant Voronoi polyhedra in $Al_{67}Mg_{33}$ with temperature.

The two calculation methods, i.e., the five-fold symmetry and ICO order from BOO parameters, give almost the same changing tendency of structure evolution in these compositions. At high temperatures, the five-fold local symmetry and ICO fraction monotonically increase with increasing Al concentration. As the temperature decreases, the five-fold local symmetry and ICO fraction significantly increase for x_{Al}=50%, 67%, 85%, and 100% compositions, with a slight increase observed for x_{Al}=15% and 33% cases. This indicates that the icosahedral order in Al−Mg melts grows up with decreasing temperature. Especially, the icosahedral order increases rapidly at x_{Al}=67% below 650 K, which is the onset point of the non-Arrhenius transition in this composition. And more interestingly, the population of the icosahedral order exceeds that of x_{Al}=85% melts at T<550 K. This inversion phenomenon happens at the points exactly the same as that in viscosity (Fig. 7(a)) and the maximum value of the non-Gaussian parameter (Fig. 4). Thus, there is a close relationship between the dynamic quantities such as shear viscosity and dynamic heterogeneity, and the icosahedral order structure in the Al−Mg melts. Actually, HU et al [47] have fitted the parameter of five-fold local symmetry and viscosity with temperature and found that the five-fold symmetry might be a good structural parameter for establishing the structure−property relationship. However, the finding here suggesting the subtle correlation between ICO order and slow dynamics or dynamic heterogeneity is still striking.

In liquids of x_{Al}=67% the population of most Voronoi polyhedra decreases with decreasing temperature, such as that of ⟨0,3,6,3⟩, ⟨0,2,8,1⟩, ⟨0,3,6,4⟩, ⟨0,2,8,2⟩, and ⟨0,1,10,2⟩ clusters (Fig. 7(d)). Meanwhile, the fraction of perfect icosahedra with the Voronoi index ⟨0,0,12,0⟩ rapidly increases, becoming the highest fraction of Voronoi polyhedron below 580 K. This indicates that the

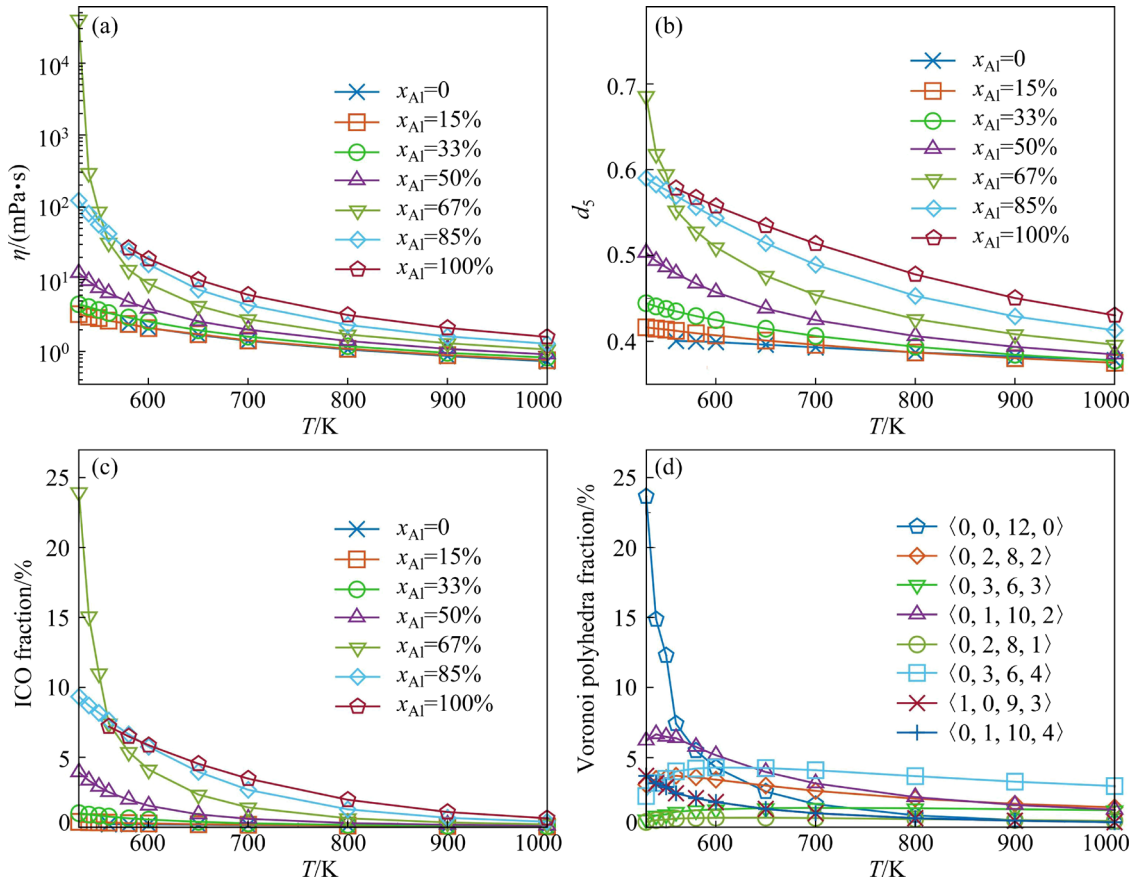

Fig. 7 Temperature evolution of viscosity (a), average degree of five-fold symmetry (b), and ICO fraction (c) in Al−Mg melts, and fraction of Voronoi polyhedra in liquids of x_{Al}=67% (d)

growth of icosahedral order in Al−Mg melts primarily originates from the increase of perfect icosahedra with the Voronoi index ⟨0,0,12,0⟩. This increment might be due to other Voronoi polyhedra transforming into ⟨0,0,12,0⟩, e.g., the transformation of distorted icosahedra indexed as ⟨0,2,8,1⟩, ⟨0,2,8,2⟩, and ⟨0,1,10,2⟩.

As more clusters transform into icosahedral clusters, the configuration entropy of the liquids could reduce with cooling down. To verify this, we calculated the local configurational entropy in different compositions. The Shannon entropy (S) in terms of Voronoi clusters can be defined as [57]

$$S=-\sum_{i=1}^{N}P_i \lg P_i \tag{14}$$

When there is only one type of Voronoi polyhedron in the liquid, with P_i=1 for that polyhedron and P_i=0 for all other types, then S=0, indicating that the system is in the most ordered structural configuration. When all Voronoi polyhedra occur with equal probability in the liquid, i.e., P_i=1/N or all types, then S reaches its maximum value, indicating that the system is in the most disordered structure.

Figure 8(a) shows the calculated Shannon entropy with temperature in different compositions. Except for pure Mg, compositions with higher icosahedral order exhibit lower local configurational entropy, and their rate of decrease is faster. This suggests that the liquids of more icosahedral clusters can also be in a more ordered structure. This phenomenon is particularly pronounced in liquids of x_{Al}=67%. At 560 K, the rate of decrease in the local configurational entropy suddenly increases in this alloy. The rapid decrease in Shannon entropy with decreasing temperature also indicates the presence of a strong non-entropic mixing effect. The same trend is observed in the Voronoi polyhedron fraction (Fig. 7(d)): the fraction of ⟨0,0,12,0⟩ rapidly increases at 560 K. This validates that the increase in the perfect icosahedral structure is due to the transformation of other types of Voronoi polyhedra into ⟨0,0,12,0⟩. This leads to a more ordered liquid structure in this composition.

By finding the drastic increment of icosahedral

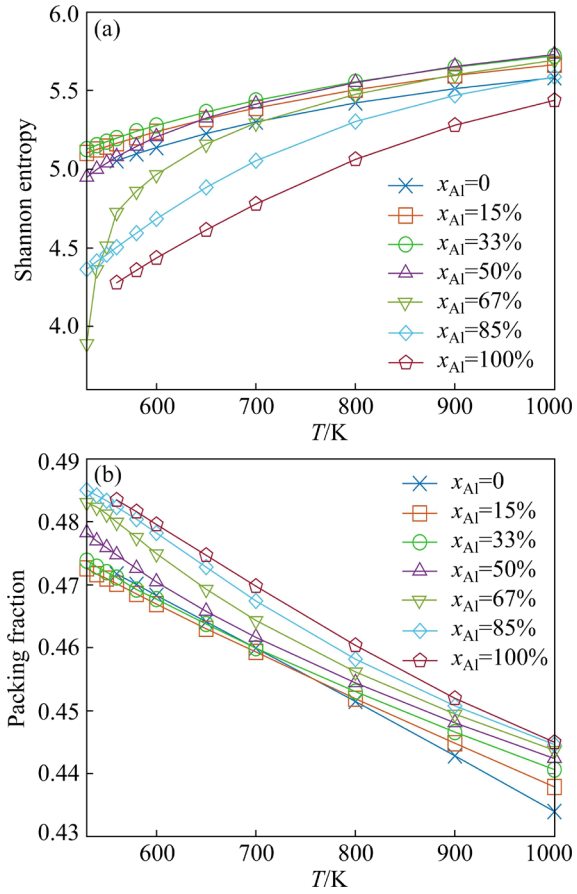

Fig. 8 Temperature evolution of local Shannon (configurational) entropy (a) and packing fraction (b)

clusters and the corresponding decrease in Shannon entropy, we concluded that the unexpected slow dynamics in liquids of x_{Al}=67% can be ascribed to the change of local structure. An intriguing question is whether there is a clue in global structural quantities that account for the dynamic changes in these liquids. One of the most prevailing methods to characterize the liquid structure is the packing fraction. This comes from the hard-sphere approximation. If the structure is more densely packed, the dynamics will be more viscous, and vice versa.

By assigning an atomic size to each atom, the global packing fraction, φ, of the liquids can be calculated by $\varphi=\rho_n \sum_\alpha c_\alpha d_\alpha^3 \pi/6$ where ρ_n is the number density and d_α is the assigned diameter of atomic species α. Figure 8(b) shows the packing fraction calculated by taking the nearest-neighbor distance from the pair distribution function as d_α. As the temperature decreases, the packing fraction increases, indicating more closely packed structure at low temperatures as expected. At the same temperature, it can be observed that the packing fraction almost monotonically increases with the increase of Al concentration. This behavior does not conform to the abnormal change of viscosity, which shows a maximum at the composition x_{Al}=67% at low temperatures. Therefore, the dynamic behavior of the melts cannot be explained in terms of the hard-sphere like approximation, but should take account of the chemical effect on the structure.

Although we find that the drastic increment of icosahedral clusters accounts for the corresponding increase of viscosity in these melts, the reason why the icosahedral order is the highest in the mediate composition, i.e., x_{Al}=67%, is still unclear. We argue that this is due to the interplay between the chemical order and the geometrical order. Figure 9 shows the fractions of eight Voronoi polyhedra in different compositions at 530 K, typically including the perfect icosahedra ⟨0,0,12,0⟩, the distorted icosahedra such as ⟨0,2,8,2⟩, ⟨0,1,10,2⟩, and ⟨1,0,9,3⟩, as well as other four large clusters that are of more coordination numbers. It can be found that the icosahedral clusters are mostly Al-centered, while the large clusters tend to be Mg-centered. When the Mg concentration is too few in the compositions, e.g., at x_{Al}=85%, the large clusters transit to be Al-centered, such as ⟨0,3,6,4⟩ and ⟨0,2,8,4⟩, or reduce their population, such as ⟨0,1,10,4⟩ and ⟨0,0,12,4⟩.

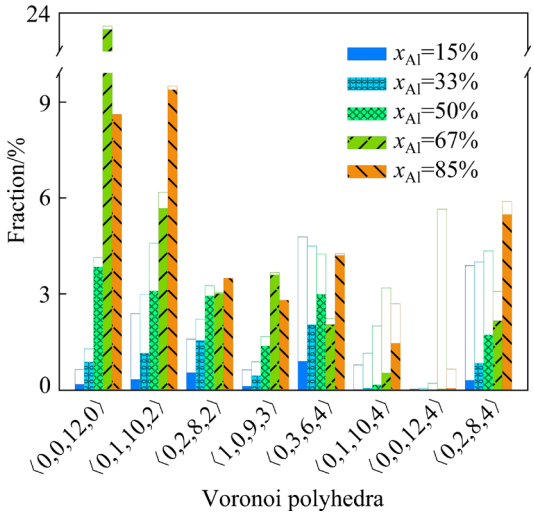

Fig. 9 Fraction of Voronoi clusters centered by Al (fulfilled squares) and Mg (hollowed squares) at 530 K (In order to clearly compare the data in different compositions, *y*-axis is broken to skip range from about 10 to 22.5)

The chemical SRO observed before is crucial for the filling efficiency of local structures. Icosahedral SRO structures have been found in Al−Mg melts [28,29,54]. The icosahedral structure, lacking translational symmetry, cannot fulfill the entire space. For an icosahedral cluster, the distance from the central atom to the atoms in the shell is 5% shorter than the distance between the atoms in the shell. The atomic radius of Al atoms is smaller than that of Mg atoms. Therefore, placing an Al atom at the center of an icosahedron and placing an appropriate number of Mg atoms in the shell can effectively increase the space utilization efficiency, forming an energetically favorable dense packing system. Thus, the chemical SRO, i.e., the preferred connection between Al and Mg is beneficial to the topological SRO, i.e., the icosahedral order.

In the icosahedral clusters, the central atoms are usually Al atoms, with Al and Mg atoms forming the shell around them. The icosahedral order can grow up with x_{Al} as more atoms can be potentially to form ICO. However, when x_{Al} is too large, the population of Mg atoms will become insufficient to adhere onto ICO cluster shells. At this time, the ICO clusters will become unstable and their population will reduce at large x_{Al}. As the temperature decreases, the proportion of icosahedra increases, and the phenomenon of Mg atom deficiency becomes more pronounced. This explains why the five-fold local symmetry and ICO fraction in the composition of x_{Al}=67% surpass those of x_{Al}=85% at 550 K.

4 Conclusions

(1) Upon cooling down, both the diffusion coefficients and viscosity of Al−Mg melts with varying compositions display an Arrhenius-to-non-Arrhenius transition at the crossover temperature, where the SE relation also breaks down. This transition is due to the emergence of slow dynamics manifested as the dynamic heterogeneity.

(2) The viscosity of $Al_{67}Mg_{33}$ surpasses that of $Al_{85}Mg_{15}$ at temperatures below 550 K. The population of the icosahedral order exhibits the same surpassing behavior in these melts at exactly the same temperature. This indicates that the subtle dynamics of the liquids is controlled by the geometrical local order.

(3) Al−Mg melts exhibit strong chemical ordering. Coordination numbers reveal that Al and Mg prefer to bond together in nearest neighbor shells. However, the Al−Mg pairs tend to repel each other in the second neighbor shells.

(4) The geometrical local order interplays with the chemical local order. The icosahedral clusters are mainly formed by the Al atoms, while a portion of Mg atoms are necessary to be in the shells of the clusters to relieve the structural frustration. The preferred heteroatomic bonding supports icosahedra formation.

CRediT authorship contribution statement

Fei-qi HUANG: Data curation, Formal analysis, Investigation, Methodology, Resources, Software, Writing – Original draft, Review & editing; **Xiao-dan WANG:** Data curation; **Lin-si-tong HUANG:** Formal analysis; **Ju-rui MA:** Investigation; **Yu-jun JIANG:** Software; **Hua-shan LIU:** Writing – Original draft, Review & editing; **Jin-liang HU:** Conceptualization, Funding acquisition, Investigation, Project administration, Resources, Supervision, Writing – Original draft, Review & editing; **Hai-long PENG:** Conceptualization, Funding acquisition, Investigation, Project administration, Resources, Supervision, Writing – Original draft, Review & editing; **Bo ZHANG:** Resources, Supervision, Writing – Original draft, Review & editing.

Declaration of competing interest

The authors declare that they have no known competing financial interests or personal relationships that could have appeared to influence the work reported in this paper.

Acknowledgments

This work was supported by the Open Research Fund of Songshan Lake Materials Laboratory, China (No. 2022SLABFN14), Guangdong Basic and Applied Basic Research Foundation, China (No. 2021A1515110108), and the National Natural Science Foundation of China (No. 52371168).

References

[1] ZHAO Juan-gang, LIU Zhi-yi, BAI Song, ZENG Di-ping, LUO Lei, WANG Jian. Effects of natural aging on the formation and strengthening effect of G. P. zones in a retrogression and re-aged Al−Zn−Mg−Cu alloy [J]. Journal

of Alloys and Compounds, 2020, 829: 154469.

[2] ZHANG Ke-long, LI Hui-zhong, LIANG Xiao-peng, CHEN Zhi, ZHAO Zi-xuan, TAO Hui, ZHOU Xiong-wen. Effect of aging time on discontinuous precipitates, continuous precipitates and mechanical properties of AZ80A magnesium alloy [J]. Transactions of Nonferrous Metals Society of China, 2022, 32(9): 2838−2851.

[3] LIU Fei, LIU Zhi-yi, JIA Peng-xiang, BAI Song, YAN Peng-fei, HU Yang-cheng. Dynamic dissolution and texture evolution of an Al−Cu−Mg−Ag alloy during hot rolling [J]. Journal of Alloys and Compounds, 2020, 827: 154254.

[4] LI Kai, CHEN Zhi-yong, CHEN Tao, SHAO Jian-bo, WANG Ren-ke, LIU Chu-ming. Hot deformation and dynamic recrystallization behaviors of Mg−Gd−Zn alloy with LPSO phases [J]. Journal of Alloys and Compounds, 2019, 792: 894−906.

[5] ZHANG Jing-yang, ZHOU Zi-qing, ZHANG Zhi-bo, PARK M H, YU Qing, LI Zi, MA Jiang, WANG An-ding, HUANG Huo-geng, SONG Min, GUO Bai-song, WANG Qi, YANG Yong. Recent development of chemically complex metallic glasses: From accelerated compositional design, additive manufacturing to novel applications [J]. Materials Futures, 2022, 1(1): 012001.

[6] SCHROERS J, PATON N. Processing of bulk metallic glass [J]. Advanced Materials, 2010, 22(14): 1566−1597.

[7] HAN Jia-jia, WANG Cui-ping, YANG Shui-yuan, LU Yong, LIU Xiang-jun. Abnormal orderly transformation in supercooled state of an Al-based alloy [J]. Physical Review Materials, 2020, 4(9): 093608.

[8] JAKSE N, PASTUREL A. Relationship between structural and dynamic properties of Al-rich Al−Cu melts: Beyond the Stokes−Einstein relation [J]. Physical Review B, 2016, 94(22): 224201.

[9] WANG Qing, SHANG Ying-hui, YANG Yong. Quenched-in liquid in glass [J]. Materials Futures, 2023, 2(1): 017501.

[10] LIU Fei, LIU Zhi-yi, JIA Peng-xiang. Effect of *T*-phase on microstructure of the hot rolled Al−Cu−Mg alloy [J]. Journal of Alloys and Compounds, 2020, 825: 154190.

[11] LIN Liang-hua, LIU Zhi-yi, LIU Wen-juan, ZHOU Ya-ru, HUANG Tian-tian. Effects of Ag addition on precipitation and fatigue crack propagation behavior of a medium-strength Al−Zn−Mg alloy [J]. Journal of Materials Science & Technology, 2018, 34(3): 534−540.

[12] JAKSE N, NGUYEN T L T, PASTUREL A. Local order and dynamic properties of liquid Au_xSi_{1-x} alloys by molecular dynamics simulations [J]. The Journal of Chemical Physics, 2012, 137(20): 204504.

[13] PASTUREL A, JAKSE N. Role of five-fold symmetry in undercooled Al−Cu binary alloys [J]. Journal of Applied Physics, 2018, 123(14): 145103.

[14] JAKSE N, PASTUREL A. Relationship between structure and dynamics in liquid $Al_{1-x}Ni_x$ alloys [J]. The Journal of Chemical Physics, 2015, 143(8): 084504.

[15] PENG Hai-long, YANG Fan, LIU Shi-tong, HOLLAND-MORITZ D, KORDEL T, HANSEN T, VOIGTMANN T. Chemical effect on the structural and dynamical properties in Zr−Ni−Al liquids [J]. Physical Review B, 2019, 100(10): 104202.

[16] PENG Hai-long, VOIGTMANN T, KOLLAND G, KOBATAKE H, BRILLO J. Structural and dynamical properties of liquid Al−Au alloys [J]. Physical Review B, 2015, 92(18): 184201.

[17] MARET M, POMME T, PASTUREL A, CHIEUX P. Structure of liquid $Al_{80}Ni_{20}$ alloy [J]. Physical Review B, 1990, 42(3): 1598−1604.

[18] FENG Yun, FENG Yan, LI Zong-bo, PENG Hai-long. Chemically ordered structure and dynamics in $Al_{80}Ti_{20}$ liquids [J]. Computational Materials Science, 2023, 226: 112256.

[19] LI Fu-dong, LIU Zhi-yi, WU Wen-ting, XIA Peng, YING Pu-you, ZHAO Qi, LI Jun-lin, BAI Song, YE Cheng-wu. On the role of texture in governing fatigue crack propagation behavior of 2524 aluminum alloy [J]. Materials Science and Engineering A, 2016, 669: 367−378.

[20] BAI Song, LIU Zhi-yi, YING Pu-you, WANG Jian, WANG An. Quantitative study of the solute clustering and precipitation in a pre-stretched Al−Cu−Mg−Ag alloy [J]. Journal of Alloys and Compounds, 2017, 725: 1288−1296.

[21] BAI Song, LIU Zhi-yi, YING Pu-you, WANG Jian, LI Jun-lin. Investigation of modulus hardening of various co-clusters in aged Al−Cu−Mg−Ag alloy by atom probe tomography [J]. Materials Science and Engineering A, 2016, 668: 234−242.

[22] TU Wen-bin, TANG Jian-guo, ZHANG Yong, YE Ling-ying, LIU Sheng-dan, LU Jin-kun, ZHAN Xin, LI Cheng-bo. Effect of Sn and Cu addition on the precipitation and hardening behavior of Al−1.0Mg−0.6Si alloy [J]. Materials Science and Engineering A, 2020, 770: 138515.

[23] BAI Song, LIU Zhi-yi, ZHOU Xuan-wei, GU Yan-xia, YU Di-er. Strain-induced dissolution of Cu−Mg co-clusters and dynamic recrystallization near a fatigue crack tip of an underaged Al−Cu−Mg alloy during cyclic loading at ambient temperature [J]. Scripta Materialia, 2011, 64(12): 1133−1136.

[24] YING Pu-you, LIU Zhi-yi, BAI Song, LIU Meng, LIN Liang-hua, XIA Peng, XIA Lin-yan. Effects of pre-strain on Cu−Mg co-clustering and mechanical behavior in a naturally aged Al−Cu−Mg alloy [J]. Materials Science and Engineering A, 2017, 704: 18−24.

[25] WU Wen-ting, LIU Zhi-yi, HU Yang-cheng, LI Fu-dong, BAI Song, XIA Peng, WANG An, YE Cheng-wu. Goss texture intensity effect on fatigue crack propagation resistance in an Al−Cu−Mg alloy [J]. Journal of Alloys and Compounds, 2018, 730: 318−326.

[26] WANG Song-you, KRAMER M J, XU Ming, WU Shun-qing, HAO Shao-gang, SORDELET D J, HO Kai-ming, WANG Cai-zhuang. Experimental and ab initio molecular dynamics simulation studies of liquid $Al_{60}Cu_{40}$ alloy [J]. Physical Review B, 2009, 79(14): 144205.

[27] LIU Feng-xiang, LIU Rang-su, HOU Zhao-yang, LIU Hai-rong, TIAN Ze-an, ZHOU Li-li. Formation mechanism of atomic cluster structures in Al−Mg alloy during rapid

solidification processes [J]. Annals of Physics, 2009, 324(2): 332−342.

[28] HOU Zhao-yang, LIU Li-xia, LIU Rang-su, TIAN Ze-an, WANG Jin-guo. Short-range and medium-range order in rapidly quenched $Al_{50}Mg_{50}$ alloy [J]. Journal of Non-Crystalline Solids, 2011, 357(5): 1430−1436.

[29] WANG Chang-chun, WONG Chee-how. Short-to-medium range order of Al−Mg metallic glasses studied by molecular dynamics simulations [J]. Journal of Alloys and Compounds, 2011, 509(42): 10222−10229.

[30] YAN Zhi-huang, HUANG Fei-qi, WU Yan-xue, LIU Hua-shan, PENG Hai-long. Fast crystal growth in deeply undercooled ZrTi melts [J]. The Journal of Chemical Physics, 2024, 160(4): 044505.

[31] ZOU Peng-fei, LI Chang, HOU Zhao-yang, SUN Jia-yi, GAO Quan-hua, LI Ke-fan, WANG Zhen, DONG Ke-jun. Formation mechanism and mechanical behavior of gradient nanograin structure in directional solidified Ti_3Al alloy: Atomic-scale study [J]. Transactions of Nonferrous Metals Society of China, 2024, 34(5): 1507−1519.

[32] CHEN Han, HU Zhang, HAN Yu-xiang, CHEN Tao, LIU Chu-ming, CHEN Zhi-yong. Microstructure and mechanical properties of Mg−Gd−Y−Zn−Zr alloy plates with different initial textures after hot rolling [J]. Transactions of Nonferrous Metals Society of China, 2024, 34(6): 1804−1816.

[33] ZHAO Qi, LIU Zhi-yi, LI Sha-sha, HU Yang-cheng, BAI Song. Effect of *S* phase characteristics on the formation of recrystallization textures of an Al−Cu−Mg alloy [J]. Journal of Alloys and Compounds, 2018, 747: 293−305.

[34] POLMEAR I. Light alloys: From traditional alloys to nanocrystals [M]. Amsterdam: Elsevier, 2005.

[35] SENGUPTA S, KARMAKAR S, DASGUPTA C, SASTRY S. Breakdown of the Stokes−Einstein relation in two, three, and four dimensions [J]. The Journal of Chemical Physics, 2013, 138(12): 12A548.

[36] AFFOUARD F, DESCAMPS M, VALDES L C, HABASAKI J, BORDAT P, NGAI K L. Breakdown of the Stokes–Einstein relation in Lennard−Jones glassforming mixtures with different interaction potential [J]. The Journal of Chemical Physics, 2009, 131(10): 104510.

[37] PENG Hai-long, LIU Hua-shan, VOIGTMANN T. Nonmonotonic dynamical correlations beneath the surface of glass-forming liquids [J]. Physical Review Letters, 2022, 129(21): 215501.

[38] WU Bo-qiang, KONG Ling-ti, LI Jin-fu. Abnormal dynamic behavior and structural origin of Cu−Ag eutectic melt [J]. Acta Materialia, 2021, 207: 116705.

[39] PLIMPTON S. Fast parallel algorithms for short-range molecular dynamics [J]. Journal of Computational Physics, 1995, 117(1): 1−19.

[40] LIU Xiang-yang, ADAMS J B. Grain-boundary segregation in Al−10%Mg alloys at hot working temperatures [J]. Acta Materialia, 1998, 46(10): 3467−3476.

[41] EGELSTAFF P A. An introduction to the liquid state [M]. Amsterdam: Elsevier, 2012.

[42] RAHMAN A. Correlations in the motion of atoms in liquid argon [J]. Physical Review, 1964, 136: 405−411.

[43] FINNEY J L. A procedure for the construction of Voronoi polyhedra [J]. Journal of Computational Physics, 1979, 32(1): 137−143.

[44] SHENG H W, LUO W K, ALAMGIR F M, BAI J M, MA E. Atomic packing and short-to-medium- range order in metallic glasses [J]. Nature, 2006, 439(7075): 419−425.

[45] HUANG Li, WANG Cai-zhuang, HAO Shao-gang, KRAMER M J, HO Kai-ming. Atomic size and chemical effects on the local order of Zr_2M (M=Co, Ni, Cu, and Ag) binary liquids [J]. Physical Review B, 2010, 81(1): 014108.

[46] PENG Hai-long, LI Mao-zhi, WANG Wei-hua. Structural signature of plastic deformation in metallic glasses [J]. Physical Review Letters, 2011, 106(13): 135503.

[47] HU Yuan-chao, LI Fu-xiang, LI Mao-zhi, BAI Hai-yang, WANG Wei-hua. Five-fold symmetry as indicator of dynamic arrest in metallic glass-forming liquids [J]. Nature Communications, 2015, 6(1): 8310.

[48] STEINHARDT P J, NELSON D R, RONCHETTI M. Bond-orientational order in liquids and glasses [J]. Physical Review B, 1983, 28(2): 784−805.

[49] PUERTAS A M, VOIGTMANN T. Microrheology of colloidal systems [J]. Journal of Physics: Condensed Matter, 2014, 26(24): 243101.

[50] HAN Xiu-jun, SCHOBER H R. Transport properties and Stokes−Einstein relation in a computer-simulated glass-forming $Cu_{33.3}Zr_{66.7}$ melt [J]. Physical Review B, 2011, 83(22): 224201.

[51] HAN Xiu-jun, LI Jian-guo, SCHOBER H R. High temperature breakdown of the Stokes-Einstein relation in a computer simulated Cu−Zr melt [J]. The Journal of Chemical Physics, 2016, 144(12): 124505.

[52] QIN Jing-yu, BIAN Xiu-fang, SLIUSARENKO S I, WANG Wei-min. Pre-peak in the structure factor of liquid Al−Fe alloy [J]. Journal of Physics: Condensed Matter, 1998, 10(6): 1211−1218.

[53] VOIGTMANN T, MEYER A, HOLLAND-MORITZ D, STUBER S, HANSEN T, UNRUH T. Atomic diffusion mechanisms in a binary metallic melt [J]. Europhysics Letters, 2008, 82(6): 66001.

[54] WANG Lu-hong, LIU Hao-zhe. The microstructural evolution of $Al_{12}Mg_{17}$ alloy during the quenching processes [J]. Journal of Non-Crystalline Solids, 2006, 352(26/27): 2880−2884.

[55] WU Shun-qing, WANG Cai-zhuang, HAO Shao-gang, ZHU Zi-zhong, HO Kai-ming. Energetics of local clusters in $Cu_{64.5}Zr_{35.5}$ metallic liquid and glass [J]. Applied Physics Letters, 2010, 97(2): 021901.

[56] NELSON D R, SPAEPEN F. Polytetrahedral order in condensed matter [J]. Solid State Physics, 1989, 42: 1−90.

[57] PENG Hai-long, LI Mao-zhi, WANG Wei-hua. Stress-versus temperature-induced structural evolution in metallic glasses [J]. Applied Physics Letters, 2013, 102(13): 131908.

Al−Mg 熔体中结构控制的慢动力学

黄非奇[1,2]，王晓丹[1]，黄林思彤[1]，马琚睿[1]，姜雨君[1]，刘华山[1]，胡金亮[2]，彭海龙[1]，张 博[2]

1. 中南大学 材料科学与工程学院，长沙 410083；
2. 松山湖材料实验室 空间材料团队，东莞 523808

摘 要：采用分子动力学模拟方法研究了 Al 成分变化的 Al−Mg 熔体的动力学和结构特性。研究结果表明：在温度低于 550 K 时，$Al_{67}Mg_{33}$ 的黏度异常地超越了 $Al_{85}Mg_{15}$ 的黏度，这与高温下的趋势不一致。二十面体有序结构的演变是导致这种异常动力学行为的原因。结构分析显示：Al 和 Mg 原子在最近邻壳层中表现出优先键合，而在第二近邻壳层中表现出排斥趋势，导致部分静态结构因子中出现预峰；由于缺少足够的 Mg 原子来稳定二十面体团簇，二十面体团簇的形成在富 Al 熔体中被抑制。该结果展示了由几何密堆与化学作用之间相互影响所导致的结构演变行为。这些发现对于理解 Al−Mg 熔体的结构−动力学性质具有重要意义。

关键词：Al−Mg 熔体；慢动力学；化学有序结构；拓扑有序结构；分子动力学模拟

(Edited by Wei-ping CHEN)